# Topological transitions for lattice bosons in a magnetic field

**Sebastian D. Huber[a,1] and Netanel H. Lindner[b,c]**

[a]Department of Condensed Matter Physics, The Weizmann Institute of Science, Rehovot, 76100, Israel; [b]Institute for Quantum Information, California Institute of Technology, Pasadena, CA 91125; and [c]Department of Physics, California Institute of Technology, Pasadena, CA 91125

Edited by Allan H. MacDonald, University of Texas at Austin, Austin, TX, and approved September 12, 2011 (received for review July 7, 2011)

**The Hall response provides an important characterization of strongly correlated phases of matter. We study the Hall conductivity of interacting bosons on a lattice subjected to a magnetic field. We show that for any density or interaction strength, the Hall conductivity is characterized by an integer. We find that the phase diagram is intersected by topological transitions between different values of this integer. These transitions lead to surprising effects, including sign reversal of the Hall conductivity and extensive regions in the phase diagram where it acquires a negative sign, which implies that flux flow is reversed in these regions—vortices there flow upstream. Our findings have immediate applications to a wide range of phenomena in condensed matter physics, which are effectively described in terms of lattice bosons.**

vortex dynamics | two-dimensional superfluids | Berry's phase | Bose–Hubbard model | Chern numbers

The Hall response is a key theoretical and experimental tool for characterizing emergent charge carriers (1) in strongly correlated systems, ranging from high temperature superconductors (2–4) to the quantum Hall effect (5). In this paper, we study the Hall conductivity of strongly correlated bosons on a lattice. We find that the entire phase diagram of such systems can be characterized using an integer $p$, and inevitably contains topological transitions between regions with different values of $p$. These observations allow us to calculate the Hall conductivity throughout the whole phase diagram, and we show that they lead to surprising consequences, such as sign reversals of the Hall conductivity. The model we study describes a wide range of systems in condensed matter physics, to which our results have immediate implications. Examples are cold atoms on optical lattices (6, 7), Josephson junction arrays (8), granular superconductors (9, 10), and perhaps even high temperature superconductors such as the underdoped cuprates (11–13).

In the absence of disorder and at weak magnetic fields the Hall conductivity of bosonic systems is dominated by the flow of superfluid vortices. For a continuum (Galilean invariant) superfluid, vortex flow gives a Hall conductivity that is proportional to the ratio of the particle density and the applied magnetic field. We find that on the lattice, vortex dynamics is strongly modified. As a result the Hall conductivity is characterized, in addition to the particle density, by the integer $p$. We show how emergent particle-hole symmetry points in the ground-state phase diagram necessarily lead to a nontrivial behavior of this integer, and we discuss the topological transitions between different $p$ sectors. As we show, these transitions are attributed to degeneracies in the many-body spectrum, which serve as sources for the Berry curvature.

Specifically, we focus on the conventional Bose–Hubbard model (14) in two dimensions. We restrict our study to a dissipationless system, at zero temperature and without disorder. Within the phase diagram of this model we find large parameter regions corresponding to a negative Hall conductivity, $\sigma_{xy} < 0$, and reversed vortex motion where vortices flow upstream (see Fig. 1). We discuss methods to directly test these results in cold atom systems where the neutral atoms are subjected to synthetic magnetic fields introduced through rotation or phase imprinting (15, 16).

## Hall Conductivity and Vortex Motion

We begin by giving a semiclassical description of vortex dynamics in bosonic systems. A vortex moving with respect to a current experiences a force arising from the interaction of the velocity field of the vortex with the external current. This hydrodynamical force is called the Magnus force, and it acts perpendicularly to the current, as depicted in Fig. 2*A*. Similarly, a superfluid vortex (of unit vorticity) in two dimensions experiences a force

$$\mathbf{F}_{\mathrm{M}} = -2\pi\hbar n_s \mathbf{v}_s \times \hat{\mathbf{e}}_z, \qquad [1]$$

where $n_s$ is the number density of superfluid bosons, and $\mathbf{v}_s$ is their velocity. The unit vector $\hat{\mathbf{e}}_z$ is a normal to the plane.

The force $\mathbf{F}_{\mathrm{M}}$ in Eq. **1** arises from the dynamical phase (time integral of the energy) in a Lagrangian describing the superfluid. Such a Lagrangian necessarily also contains a term corresponding to the Berry phase picked up by the vortex motion. The Berry phase acquired by a vortex moving around a loop of area $S$ is given by $2\pi\alpha S$, where $\alpha$ is a proportionality factor that depends on the microscopic details of the Hamiltonian. Therefore, an equation of motion for the vortex leading to dissipationless flow is linear in the vortex velocity and given by (17)

$$\mathbf{F}_{\mathrm{M}} + 2\pi\hbar\alpha \mathbf{v}_v \times \hat{\mathbf{e}}_z = 0. \qquad [2]$$

Eq. **2** can also be understood from the perspective of momentum balance. A moving vortex imprints a phase discontinuity on the superfluid wave function. The Josephson relation $\Delta\mu = \hbar\partial_t\Delta\varphi$ connects the resulting chemical potential to the time derivative of the relative phase difference (see Fig. 2*B*). The chemical potential drop will be balanced by a flow of particles, which results in momentum transfer from the particles to the moving vortex, perpendicular to the vortex velocity $\mathbf{v}_v$ and proportional to its magnitude. The proportionality factor $\alpha$ relates the change in the system's momentum to the vortex velocity.

The Hall conductivity can be related to the drift velocity of a vortex. From Eqs. **1** and **2** we get

$$\mathbf{v}_v = \frac{n_s}{\alpha}\mathbf{v}_s. \qquad [3]$$

In a system with a low density of vortices we can neglect the effects of vortex–vortex interactions. Considering strictly dissipationless flow, we obtain from the Josephson relation a semiclassical expression for the Hall conductivity

Author contributions: S.D.H. and N.H.L. designed research, performed research, and wrote the paper.

The authors declare no conflict of interest.

This article is a PNAS Direct Submission.

[1]To whom correspondence should be addressed. E-mail: sebastian.huber@weizmann.ac.il.

This article contains supporting information online at www.pnas.org/lookup/suppl/doi:10.1073/pnas.1110813108/-/DCSupplemental.

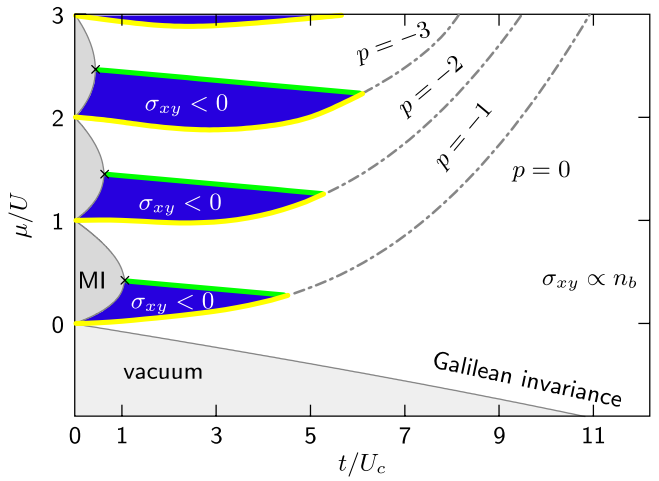


**Fig. 1.** Topological transitions in the Bose–Hubbard phase diagram. The figure overlays the ground-state phase diagram of the Bose–Hubbard model (as a function of the hopping $t/U$ and the chemical potential $\mu/U$) with a map of the topologically distinct sectors. The gray regions indicate the insulating Mott phases separated by a second-order transition from the surrounding superfluid. In the presence of a magnetic field, the superfluid (white and blue regions) has a nonvanishing Hall conductivity $\sigma_{xy} \propto n_b + p$, which is characterized by the particle density $n_b$ and the topological index $p$. The dash-dotted lines mark topological transitions between different $p$ sectors. The regions shown in blue are characterized by a negative Hall conductivity, whereas in the white regions the Hall conductivity is positive. The transition between positive and negative $\sigma_{xy}$ is smooth through the green lines and discontinuous through the yellow lines.

$$\sigma_{xy} = \frac{q n_s v_s}{\Delta\mu} = \frac{q^2 n_s v_s}{2\pi\hbar n_v v_v} = \frac{q^2}{h}\frac{\alpha}{n_v}, \qquad [4]$$

where $n_v$ is the density of vortices and $q$ is the boson charge.

In systems with Galilean invariance, in a reference frame moving at the vortex velocity, there should be no forces acting on the vortex, requiring $\mathbf{v}_v = \mathbf{v}_s$ and therefore setting $\alpha = n_s$ (18, 19). This relation is modified in the presence of a lattice, as we discuss now.

We consider the standard model for interacting bosons on a lattice (14)

$$\mathcal{H} = -t\sum_{\langle \mathbf{r},\mathbf{r}'\rangle}[b^\dagger_{\mathbf{r}} b_{\mathbf{r}'} e^{iA_{\mathbf{r}\mathbf{r}'}} + b^\dagger_{\mathbf{r}} b_{\mathbf{r}'} e^{-iA_{\mathbf{r}\mathbf{r}'}}] + \frac{U}{2}\sum_{\mathbf{r}} b^\dagger_{\mathbf{r}} b_{\mathbf{r}}(b^\dagger_{\mathbf{r}} b_{\mathbf{r}} - 1) - \mu\sum_{\mathbf{r}} b^\dagger_{\mathbf{r}} b_{\mathbf{r}}, \qquad [5]$$

where $b^\dagger_{\mathbf{r}}$ creates a boson on site $\mathbf{r}$, $t$ is the hopping amplitude, $U$ is the on-site repulsion; $A_{\mathbf{r}\mathbf{r}'} = q\int_{\mathbf{r}}^{\mathbf{r}'}\mathbf{A}\cdot\mathbf{dx}$ is the phase factor due to applied gauge field $\mathbf{A}$. We work in units where $\hbar = c = 1$, and likewise we set the lattice constant $a = 1$.

We first note that vortices live on the center of the plaquettes of the lattice. We define $2\pi\alpha$ to be the Berry phase acquired by moving a vortex around a lattice site (i.e., around a plaquette of the dual lattice).* In order to compute $\alpha$ we explicitly construct operators $\mathcal{T}_x$ and $\mathcal{T}_y$ that translate a vortex by one lattice constant in the $x$ and $y$ directions. We show that they obey the commutation relation (see *SI Text* for a full derivation)

$$\mathcal{T}_x\mathcal{T}_y = \mathcal{T}_y\mathcal{T}_x e^{2\pi i\hat{N}_b/N}. \qquad [6]$$

Here, $\hat{N}_b$ is the total boson number operator, and $N$ is the number of sites. We denote the particle filling by $n_b = N_b/N$. From Eq. **6**, we obtain

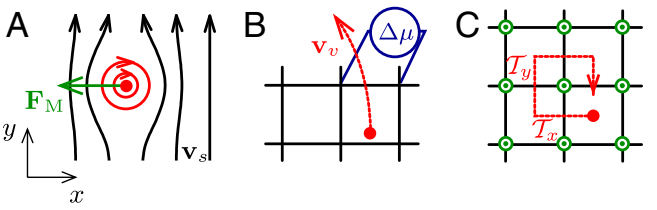


**Fig. 2.** Forces acting on a vortex. (*A*) The classical Magnus force due to the interaction of the velocity field of the vortex and the external flow $\mathbf{v}_s$ acts perpendicular to $\mathbf{v}_s$. (*B*) Vortex motion leads to a change in the momentum of the system due to its phase singularity, which is perpendicular to its velocity $\mathbf{v}_v$. (*C*) Moving a vortex around a lattice site yields a Berry phase of $2\pi\alpha = 2\pi(n_b + p)$.

$$2\pi\alpha = 2\pi(n_b + p) \quad \text{with } p \in \mathbb{Z}. \qquad [7]$$

The integer $p$ arises from the $2\pi$ ambiguity in Eq. **6**.

Eq. **7** can also be understood in terms of momentum balance (20). Following Paramekanti and Vishwanath (21), we note that Eq. **6** implies that when a vortex is transported by $\Delta y$ sites along $\hat{\mathbf{e}}_y$, the momentum of the system changes by $\Delta P_x = 2\pi n_b \Delta y$. At the same time we can integrate Eq. **2** to obtain $\Delta P_x = 2\pi\alpha\Delta y$. Combining the two results and taking into account that momentum is only conserved up to a reciprocal lattice vector $2\pi p$ leads us to Eq. **7**.

The above results, together with Eq. **4**, imply a similar relation for the Hall conductivity,

$$\sigma_{xy} n_v = \frac{q^2}{h}(n_b + p) \quad \text{with } p \in \mathbb{Z}. \qquad [8]$$

Although Eqs. **4** and **8** are a semiclassical derivation of the Hall conductivity, below we derive an *exact* relation between α and the Hall conductivity for a system containing *one vortex*,† $N_v = 1$,

$$\sigma_{xy}^{(N_v=1)} = \frac{q^2}{h}N\alpha = \frac{q^2}{h}N(n_b + p) \quad \text{with } p \in \mathbb{Z}. \qquad [9]$$

In the remainder of this paper we investigate the relations **7**–**9** throughout the phase diagram of the Bose–Hubbard model. First, we study these relations in the Gross–Pitaevskii and Mott transition limits. In the following sections we then study the transition between different $p$ sectors in the hard-core boson limit. Finally, we complete the phase diagram using numerical calculations.

## Low-Energy Limits

We start by discussing low-energy limits of Eq. **5** where a diverging length scale enables the derivation of a continuum low-energy theory. In these limits α and $\sigma_{xy}$ can be deduced directly. We review the derivation of the low-energy theories for weak ($U \ll t$) and strong ($U \gg t$) interactions. In both cases we start by rewriting Eq. **5** as a coherent state path integral with the following action for the complex valued field $\psi_i$:

$$S = \int d\tau\Big\{\sum_i \psi_i^*(\partial_\tau - \mu)\psi_i - t\sum_{\langle i,j\rangle}(\psi_i^*\psi_j e^{-i\varphi ij} + \text{c.c.}) + \frac{U}{2}\sum_i |\psi_i|^2(|\psi_i|^2 - 1)\Big\}, \qquad [10]$$

where c.c. is the complex conjugate.

**The Gross–Pitaevskii Limit.** In the weakly interacting limit, the Gross–Pitaevskii (GP) healing length $\xi_{GP} = a\sqrt{t/Un_b}$ is much larger than the lattice spacing $a$, which enables a straightforward

*The Berry phase acquired by moving a vortex around a dual plaquette is related to $\alpha$ in the semiclassical theory (see Eq. **2**), by dividing by the area of a plaquette $a^2$.

†Note that the exact relation in Eq. **9** is related to Eq. **8** by setting $n_v = 1/N$.

gradient expansion of Eq. **10**. To lowest order in gradients we obtain the continuum action

$$S = \int d\tau d\mathbf{x}\{\psi^* \partial_\tau \psi + a^2 t|(\nabla - iq\mathbf{A})\psi|^2 + \cdots\}. \qquad [11]$$

Using the above expression we can now derive the coefficient $\alpha$ in the Gross–Pitaevskii limit. When written in terms of $\psi = \sqrt{n_b}\exp(i\vartheta)$, the term $\psi^*\partial_\tau\psi$ in Eq. **11** leads to a purely imaginary $\mathscr{L}_\tau = 2\pi i m n_b$, where $m$ is a field that counts the winding of the phase $\vartheta$ (17). Consider the action of a field configuration associated with taking a vortex around a closed loop of area $S$. A little reflection shows that the regions outside the loop do not change the value of $m$, whereas those inside contribute unity per particle. Hence, $\mathscr{L}_\tau$ gives rise to a Berry phase of $2\pi i n_b S$ (18). This observation fixes

$$\alpha = n_b. \qquad [12]$$

**Around the Mott Insulator.** At strong interactions and integer filling, $n_b \in \mathbb{N}$, the Hamiltonian (Eq. **5**) stabilizes a localized Mott insulating phase with vanishing superfluid fraction $\bar{\psi}_i \equiv \langle \psi_i \rangle = 0$ (14). In the insulating phase, all sites are occupied by exactly $n_b$ bosons. Both the addition or removal of a particle is protected by a finite gap. This gap closes at the boundary of the Mott lobes in the phase diagram of Fig. 1, whereby at the lower (upper) boundary of the Mott lobe the hole (particle) gap vanishes. Hence, the tip of the Mott lobe represents a multicritical point where the particle and hole gap close simultaneously (22). In the following, we focus on this multicritical point.

When both the particle and hole gap vanish, an enhanced symmetry in the low-energy sector emerges. Instead of going through the standard procedure of deriving the low-energy theory from microscopic considerations (23, 24), we motivate the effective action via its symmetry properties. We expect the following particle-hole symmetry (PHS) to hold $\bar{\psi} \to \bar{\psi}^*$ and $\mathbf{A} \to -\mathbf{A}$ (25). To leading order in powers of $\bar{\psi}$ we find

$$S = \int d\tau d\mathbf{x}\left\{\frac{1}{8tn_b}|\partial_\tau\bar{\psi}|^2 + a^2 t n_b|(\nabla - iq\mathbf{A})\bar{\psi}|^2 + \cdots\right\}. \qquad [13]$$

The gradient expansion leading to an effective continuum theory is controlled by the diverging correlation length close to the second-order phase transition into the Mott insulating state.

A direct consequence of PHS in the *continuum theory* (Eq. **13**) is $\sigma_{xy}(\mathbf{A}) = \sigma_{xy}(-\mathbf{A})$. Together with the Onsager relation $\sigma_{xy}(\mathbf{A}) = -\sigma_{xy}(-\mathbf{A})$ we obtain $\sigma_{xy} = 0$. This result can also be understood in terms of vortex motion. As opposed to the Gross–Pitaevskii action, the continuum theory (Eq. **13**) is real. Hence it does not give rise to any Berry phase when a vortex is moved around a closed loop, and we conclude

$$\alpha = 0. \qquad [14]$$

Starting from the PHS points, we expect to find lines with $\alpha = 0$ in the $\mu/U - t/U$ phase diagram of the Bose–Hubbard model. From Eq. **7**, on the other hand, we know that at a fixed density, $\alpha$ can only change by an integer, which leads to the conclusion that the lines with $\alpha = 0$ are bound to lines of integer fillings in the phase diagram (see Fig. 1).

## Hard-Core Bosons Limit

We now consider the limit $t/U \to 0$ and $\mu/U \to m$, where $m$ is an integer. In Fig. 1, these limits lie in-between two Mott lobes. The two states with $m$ and $m+1$ bosons per site are degenerate single-site states of the Hamiltonian [**5**]. States with different fillings are separated by a gap of order $U$ and do not appear in the low-energy theory.

We use a Schrieffer–Wolf transformation (26) to project the Hamiltonian [**5**] onto the subspace with only $m$ and $m+1$ bosons per site. The resulting Hamiltonian corresponds to hard-core bosons (HCB) and can be written using spin-half operators; $S_i^z + \frac{1}{2}$ is the on-site number operator, and $S_i^+$ ($S_i^-$) raises (lowers) the occupation by one. At zeroth order in $t/U$, the HCB Hamiltonian is given by

$$\mathscr{H}_{\mathrm{HC}}^{(0)} = -(m+1)t\sum_{\langle \mathbf{r},\mathbf{r}'\rangle}(e^{iA_{\mathbf{r}\mathbf{r}'}}S_{\mathbf{r}}^+ S_{\mathbf{r}'}^- + \mathrm{h.c.}) - \mu\sum_{\mathbf{r}} S_{\mathbf{r}}^z, \qquad [15]$$

where h.c. represents the hermitian conjugate.

The HCB Hamiltonian Eq. **15** has an emergent charge conjugation symmetry. One defines the unitary transformation

$$C \equiv \exp\left(i\pi\sum_{\mathbf{r}} S_{\mathbf{r}}^x\right). \qquad [16]$$

$C$ transforms particles into holes (i.e., $C^\dagger S_{\mathbf{r}}^z C = -S_{\mathbf{r}}^z$), and

$$C^\dagger \mathscr{H}_{\mathrm{HC}}^{(0)}(q\mathbf{A},\mu)C = \mathscr{H}_{\mathrm{HC}}^{(0)}(-q\mathbf{A},-\mu). \qquad [17]$$

At half-filling for the hard-core bosons, the Hamiltonian [**15**] is independent of $\mu$ and hence Eq. **17** implies invariance under $\mathbf{A} \to -\mathbf{A}$. Hence, the Onsager relation $\sigma_{xy}(\mathbf{A}) = -\sigma_{xy}(-\mathbf{A})$ implies that for half-integer fillings ($n_b = \frac{1}{2} + m$)

$$\sigma_{xy} = \alpha = 0. \qquad [18]$$

Note that the situation at the HCB limits and at the tip of the Mott lobes are qualitatively different. The Hall conductivity at the tip of the Mott lobe vanishes due to a zero crossing of $\alpha$ when $p = -n_b$. In the HCB limit, the integer $p$ jumps exactly at $n_b = m + \frac{1}{2}$. In other words, in the first case it reflects a particle-hole-symmetry between $n_b - 1$ and $n_b + 1$, whereas in the latter, the symmetry connects $n_b - 1$ and $n_b$ at $n_b = m + \frac{1}{2}$. The symmetry at the HCB limits has a remarkable consequence for $\sigma_{xy}$ in the full phase diagram of the model, as we shall now show.

## Away from the Hard-Core Boson Limit

We now consider the effect of a finite but small value of $t/U$. Second-order processes in which a virtual excitation with an on-site occupation of $m-1$ or $m+2$ bosons are created lead to corrections to the HCB Hamiltonian [**15**] of order $t^2/U$. Taking into account all the different processes, we obtain up to irrelevant renormalizations of the parameters in $\mathscr{H}_{\mathrm{HC}}$

$$\mathscr{H}_{\mathrm{HC}}^{(1)} = \mathscr{H}_{\mathrm{HC}}^{(0)} - \epsilon_m \sum_{\langle\langle \mathbf{r},\mathbf{r}';\mathbf{r}''\rangle\rangle}\left[e^{iA_{\mathbf{r}\mathbf{r}'}}S_{\mathbf{r}}^+ S_{\mathbf{r}'}^-\left(S_{\mathbf{r}''}^z + \frac{1}{2}\right) + \mathrm{h.c.}\right], \qquad [19]$$

where $\langle\langle \mathbf{r},\mathbf{r}';\mathbf{r}''\rangle\rangle$ denote sites $\mathbf{r}$ and $\mathbf{r}'$ which are nearest neighbors of site $\mathbf{r}''$, and $\epsilon_m = (m+1)(m+2)t^2/U$.

The new terms in Eq. **19** break the charge conjugation symmetry. Therefore, for finite $t/U$, the Hall conductivity at exactly half integer filling does not vanish; below we calculate it in the limit of small $t/U$.

We consider the model Eq. **19** on a torus of size $N = L_x L_y$, with $N$ even. The gauge field $\mathbf{A}$ describes a uniform flux penetrating the surface of the torus. We take the total flux to be one flux quantum, which induces one vortex into the system. An important gauge invariant quantity described by the gauge field are the two Wilson line functions (27)

$$\Phi_x(y) = \oint dx A_x, \qquad \Phi_y(x) = \oint dy A_y. \qquad [20]$$

We define $\Theta_x = \Phi_x(y=0)$ and $\Theta_y = \Phi_y(x=0)$. Changing the values of $\Theta_x$ and $\Theta_y$ corresponds to threading Aharonov–Bohm (AB) fluxes through the two holes of the torus (27).

The Hall conductivity at zero temperature for a general many-body Hamiltonian can be calculated by integrating the Berry

curvature (28)

$$\sigma_{xy} = \frac{q^2}{h}\frac{1}{2\pi}\int_0^{2\pi} d\Theta_x \int_0^{2\pi} d\Theta_y \mathcal{F}. \qquad [21]$$

$\mathcal{F}$ is given by

$$\mathcal{F} = \epsilon^{\mu\nu}\partial_{\Theta_\mu}\mathcal{A}_\nu, \qquad \mathcal{A}_\nu = i\left\langle \Psi_0(\mathbf{\Theta})\middle|\frac{\partial\Psi_0(\mathbf{\Theta})}{\partial\Theta_\nu}\right\rangle. \qquad [22]$$

Here $\Psi_0(\mathbf{\Theta})$ is the many-body ground-state wave function that depends on the AB fluxes through the holes of the torus.

Remarkably, the Hall conductivity in the presence of one vortex can be calculated analytically at half-filling. The key ingredients are degeneracies in the spectrum that occur for $t/U = 0$ (27, 29) and serve as point (monopole) sources for the Berry curvature $\mathcal{F}$ (30).

To understand the degeneracies, we consider an effective Hamiltonian for the vortex hopping between dual lattice sites. As shown in refs. 27 and 29, this Hamiltonian is given by

$$\mathcal{H}_V = -t_V \sum_{\langle \mathbf{R},\mathbf{R}'\rangle} (e^{iA^D_{\mathbf{R},\mathbf{R}'}} b^\dagger_{\mathbf{R}} b_{\mathbf{R}'} + \text{h.c.}) + \sum_{\mathbf{R}} U(\mathbf{R}-\mathbf{R}_V) b^\dagger_{\mathbf{R}} b_{\mathbf{R}}, \quad [23]$$

where $b^\dagger_{\mathbf{R}}$ creates a vortex on a dual lattice site, and $t_V \approx t$. The dual gauge field's flux is given by the boson density, $\nabla\times\mathbf{A}^D = \Phi^D = 2\pi n_b$. The potential $U(\mathbf{R}-\mathbf{R}_V)$ for the vortex position arises due to the fact that the Wilson lines [**20**] break translational symmetry on the torus. In fact, as shown in refs. 27 and 29, for one flux quantum penetrating the surface of the torus, all translational symmetries are absent, and the potential $U(\mathbf{r}-\mathbf{R}_V)$ acquires its minimum at a point $\mathbf{R}_V$ for which the Wilson lines both take on the value $\pi$.

If the point $\mathbf{R}_V$ lies on a site of the direct lattice, the eigenstates of $\mathcal{H}_V$ (in a symmetric gauge) can be written as $\psi(\mathbf{R}-\mathbf{R}_V) = f(|\mathbf{R}-\mathbf{R}_V|)e^{im\varphi(\mathbf{R}-\mathbf{R}_V)}$. Here $\varphi(\mathbf{R}-\mathbf{R}_V)$ denotes the angle between $\mathbf{R}-\mathbf{R}_V$ and the $x$ axis, and $m = 0, \pm1, \pm2$. At half-filling, the average dual flux per plaquette is $\overline{\Phi}_D = \pi$ and the ground state is doubly degenerate with $m = 0,1$. The two states $|R\rangle$ ($m = 0$) and $|L\rangle$ ($m = 1$) represent states with clockwise and counterclockwise vortex currents, respectively, as depicted in Fig. 3*B*. Note that this twofold degeneracy occurs for $N$ distinct values of $\mathbf{\Theta}$.

To calculate $\sigma_{xy}$, we need to analyze the spectrum around the $N$ degeneracy points. Around these points, the Hamiltonian restricted to the $|R\rangle$ and $|L\rangle$ basis is of the form $H_V = \mathbf{h}\cdot\boldsymbol{\sigma}$, where

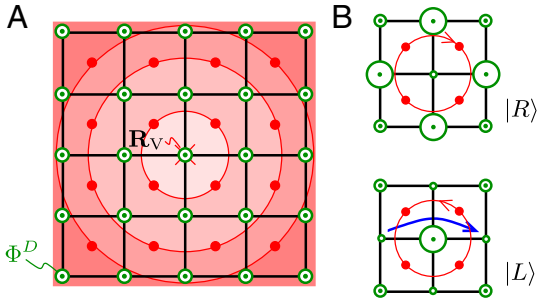


**Fig. 3.** Vortex Hamiltonian. (*A*) The vortex hops between dual lattice sites (red), where at half-filling for the bosons the average dual flux per plaquette, $\Phi^D$, is one-half of a flux quantum. The circular contours represent the equipotential contours for the confining potential for the vortex. When the Aharonov–Bohm fluxes are tuned to $\Theta^0_x$, $\Theta^0_y$ the minimum of the potential is situated on a (direct) lattice site and the vortex ground state has two degenerate states $|R\rangle$, $|L\rangle$. (*B*) The two ground states correspond to two different charge density wave configurations, with $|R\rangle$ ($|L\rangle$) corresponding to depleted (excess) charge at $\mathbf{R}_V$. When the particle-hole symmetry breaking terms of Eq. **19** are introduced, hopping terms through $\mathbf{R}_V$ (depicted by the blue arrow) lower the energy of the state $|L\rangle$ relative to $|R\rangle$.

$\boldsymbol{\sigma}$ are the pauli matrices. To find $\mathbf{h}$, we first notice that if $\mathbf{\Theta}^0 = (\Theta^0_x,\Theta^0_y)$ is a degeneracy point, tuning away from it by $\mathbf{\Theta} = \mathbf{\Theta}^0 + \Delta\mathbf{\Theta}$, moves $\mathbf{R}_V$ as (27)

$$\mathbf{R}_V = \mathbf{R}^0_V + \Delta\mathbf{R}_V, \qquad \Delta R^\alpha_V = -\frac{1}{2\pi}\epsilon^{\alpha\beta}L_\alpha\Delta\Theta_\beta, \qquad [24]$$

where $\alpha,\beta = x,y$ are not summed. Thus, tuning away from $\mathbf{\Theta}^0$ breaks the degeneracy between the two ground states $|R\rangle$ and $|L\rangle$, as it shifts the minimum of the potential $U(\mathbf{R}-\mathbf{R}_V)$. Second, the terms $\propto\epsilon_m$ in [**19**] lift the degeneracy even at $\mathbf{\Theta} = \mathbf{\Theta}^0$; the assisted hopping terms through $\mathbf{R}_V$ (blue arrow in Fig. 3*B*) favor $|L\rangle$ over $|R\rangle$.

Together, these two effects give rise to the following low-energy Hamiltonian for each degeneracy point (see *SI Text* for details),

$$\mathcal{H}_V = \tilde{U}(-\Delta\Theta_y\sigma_x + \Delta\Theta_x\sigma_y) + \tilde{\epsilon}\sigma_z. \qquad [25]$$

where the energy scales appearing above are $\tilde{U} \propto \frac{\partial U}{\partial R}\frac{L_\alpha}{2\pi}$, and $\tilde{\epsilon} \propto \epsilon_m$.

We use Eqs. **21**–**25** to calculate the Hall conductivity for *one vortex*. Consider the Hamiltonian $\mathcal{H}^{(1)}_{\text{HC}}$ of Eq. **19** where we let the parameter $\epsilon_m$ take on both negative and positive values. For $0 < \epsilon_m/t \ll 1$, the many-body ground-state $\Psi_+(\mathbf{\Theta},\epsilon_m)$ is nondegenerate, and likewise $\Psi_-(\mathbf{\Theta},\epsilon_m)$ for $-1 \ll \epsilon_m/t < 0$. For $\epsilon_m = 0$, the two states become degenerate at a set of $N$ values of $\mathbf{\Theta}$ space. The Berry connection of the ground-state manifold at $\epsilon_m = 0$ is given by

$$\mathcal{A}_\mu = i\sum_{i=+,-}\left\langle \Psi_i(\mathbf{\Theta})\middle|\frac{\partial\Psi_i(\mathbf{\Theta})}{\partial\Theta_\mu}\right\rangle \qquad [26]$$

and must satisfy $\int d^2\mathbf{\Theta}\mathcal{F} = 0$ due to particle-hole symmetry at $\epsilon_m = 0$. As a result,

$$\sigma_{xy}(\epsilon_m > 0) + \sigma_{xy}(\epsilon_m < 0) = 0. \qquad [27]$$

Next, we consider the space of $\Theta_x,\Theta_y,\epsilon_m$, which has the topology of a thick torus, as depicted in Fig. 4. We are interested in the integral of the Berry curvature $\mathcal{F}$ on the surfaces with $\epsilon_m > 0$ and $\epsilon_m < 0$, which yield $\sigma_{xy}(\epsilon_m > 0)$ and $\sigma_{xy}(\epsilon_m < 0)$, respectively. At the same time, an analog of Gauss's law for $\mathcal{F}$ implies that the integral of $\mathcal{F}$ on these surfaces counts the number of sources for $\mathcal{F}$ (30, 31). These are just the degeneracy points discussed above, which are all described by Eq. **25** and therefore correspond to sources with charge $+\frac{1}{2}$, which leads to

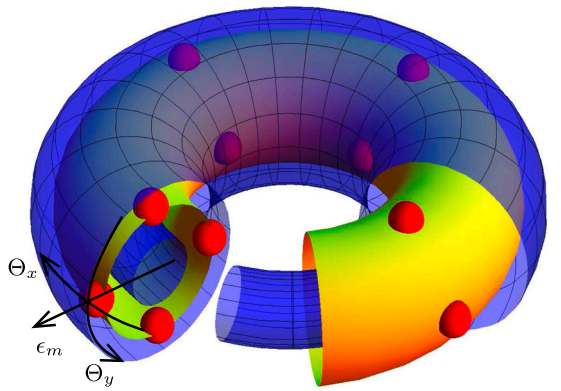


**Fig. 4.** Berry monopoles. The parameter space of $\Theta_x$, $\Theta_y$, and $\varepsilon_m$. The yellow surface denotes the particle-hole symmetric manifold $\varepsilon_m = 0$, on which the red dots denote the degeneracy points for $N$ values of $(\Theta_x,\Theta_y)$. The blue surfaces denote $\varepsilon_m < 0$ and $\varepsilon_m > 0$. The integral of the curvature $\mathcal{F}$ on these surfaces counts the number of sources in the three-dimensional parameter space which they enclose.

$$\sigma_{xy}(\epsilon_m > 0) - \sigma_{xy}(\epsilon_m < 0) = N. \quad [28]$$

Combining Eqs. **27** and **28** gives

$$\sigma_{xy}(0 < t/U \ll 1) = \frac{N}{2}. \quad [29]$$

Before concluding this section, we note that Eq. **24** leads to an exact relation between α and the Hall conductivity of one vortex. From Eq. **24**, the Berry phase for moving a vortex around a plaquette is given by

$$2\pi\alpha = \oint_{\mathscr{C}} d\Theta_\mu \mathcal{A}_\mu = \int_{S(\mathscr{C})} d^2\boldsymbol{\Theta}\mathcal{F}, \quad [30]$$

where the contour $\mathscr{C}$ defines a square of size $2\pi/L_x \times 2\pi/L_y$ in flux space, and $S(\mathscr{C})$ is the surface it bounds. Therefore, for one vortex,

$$\alpha N = \frac{1}{2\pi}\int_0^{2\pi} d\Theta_x \int_0^{2\pi} d\Theta_y \mathcal{F} = \sigma_{xy}. \quad [31]$$

Consider again the phase diagram of the Bose–Hubbard model. From the above discussion, we conclude that the transitions lines between two integer values of $p$ emanate from the HCB points and move to higher densities with increasing $t/U$. These lines all correspond to changes of the integer $p$ by unity. The PHS lines emanating from the neighboring Mott lobe tips *terminate* at these topological transition lines (see Fig. 1). Together, these two types of lines define regions with negative α and Hall conductivity.

## Evolution of the Transition Lines

We numerically calculate the Chern number (21) for one vortex, to obtain the behavior of the integer $p$ in the full parameter regime of the Bose–Hubbard model. We use a Lanczos algorithm (32) to find the ground-state wave function $\Psi_0(\boldsymbol{\Theta})$ for different AB fluxes. Using a standard procedure (33) to numerically integrate the Berry curvature [**22**] we obtain the Hall conductivity for different values of $t/U$ and $n_b$.

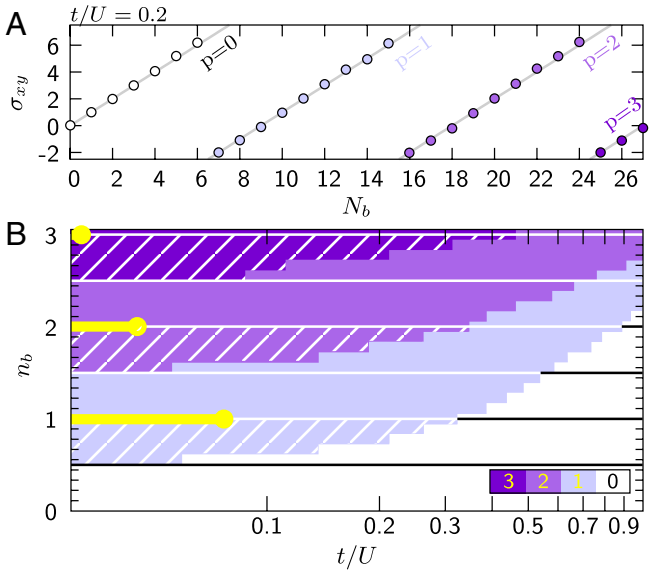


**Fig. 5.** Numerical results. (*A*) The Chern number calculated numerically on a $3 \times 3$ system at $t/U = 0.2$ for various particle numbers $N_b$. The different branches are described by different values of the integer $p$. (*B*) Phase diagram as a function of $t/U$ and $n_b$ obtained from cuts at different $t/U$, of the form in *A*. Different colors indicate the different values of the integer $p$. The lines where the integer $p$ changes by one are the topological transitions. The regions where the resulting Hall conductivity is negative is hatched in yellow. The Mott insulators at integer filling are indicated by the yellow bars.

In Fig. 5, we show the results obtained for a $3 \times 3$ cluster (see *SI Text*). We indicate which integer $p$ describes the Hall conductivity in Fig. 5*B*. Regions in the phase diagram where $\sigma_{xy} < 0$ are marked with yellow hatches. Fig. 5*A* shows a trace of $\sigma_{xy}$ for different particle numbers at $t/U = 0.2$. As expected from the calculation at half-filling, the transition lines between integer values of $p$ move to higher densities for $t/U > 0$. Remarkably, the transition lines intersect the integer density line at increasing values of $t/U$ for higher densities. As a direct consequence, the area of negative Hall conductivity *increases* for higher densities, which is in contrast to the *decreasing* extent of the Mott insulating phases indicated by the yellow bars in Fig. 5*B*. This surprising behavior of the Bose–Hubbard model is explained below.

In order to see at which values of $t/U$ a sign change of α should be expected at integer fillings, we consider the healing length $\xi_{GP}$, which sets the size of a vortex. For $\xi_{GP} = a\sqrt{t/Un_b} \ll a$, the size of a vortex is much smaller then the lattice spacing $a$ (34), and the Bose–Hubbard model maps onto the quantum rotor model (10, 35), which has an emergent PHS at integer filling (17, 36). We have seen that PHS implies $\alpha = 0$. The dependence of $\xi_{GP}$ on the *mean-field* interaction $Un_b$ therefore explains the growing extent of the negative Hall conductivity. This behavior has to be contrasted to the bosonic enhancement factors in the hopping terms $\propto\sqrt{n_b}$ which facilitate the melting of the Mott insulator and lead to smaller Mott lobes at increasing densities.

Finally, in Fig. 1 we present the numerical results as a function of $t/U$ and $\mu/U$. To translate from the results at fixed density $n_b$ to a fixed chemical potential $\mu$, we use a standard mean-field approach (37).

## Experimental Verification

Our results can be directly verified experimentally using two complimentary approaches. First, α, and in particular its sign, can be determined by directly measuring the vortex velocity. Second, the transverse response of collective modes of a superfluid can be used to measure its Hall conductivity. In the following, we discuss methods to implement these approaches in a system of cold atoms.

In the presence of a superfluid current, the vortex velocity is related to α via Eq. **3**. In a cold-atoms setup, the direction and speed of the vortex flow can be measured with in situ imaging techniques (38), which image the density profile near the vortex core. However, in the strongly interacting regime, the vortex core is on the order of the lattice spacing $a$. Hence, to make the vortex visible in the density profile, the system parameters have to be ramped into the weakly interacting regime before imaging.

The sign change of the Hall conductivity can also be detected by studying collective modes of an atomic superfluid in a harmonic trap. We illustrate the effect of the Hall conductivity on the dynamics of the "sloshing" mode (39). This mode is excited by suddenly displacing the minimum of the harmonic trap with respect to the atomic cloud. In the absence of a Hall response, this displacement causes the center of the atomic cloud to oscillate in the trap along the displacement axis, as shown in Fig. 6. A non-

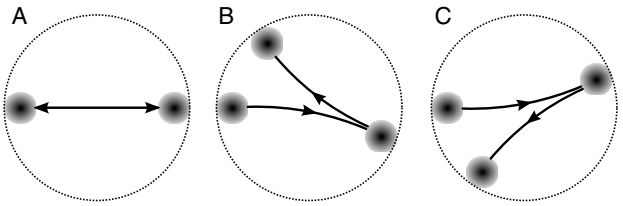


**Fig. 6.** Collective modes. Schematic map of the evolution of the center of mass of an atomic cloud in a harmonic trap. (*A*) For $\sigma_{xy} = 0$, the axis of oscillation is constant in time. (*B*) For $\sigma_{xy} > 0$, the atoms are deflected to the right leading to a rotation of the oscillation axis. (*C*) For $\sigma_{xy} < 0$, the atoms are deflected in the opposite direction.

PHYSICS

zero Hall conductivity yields a transverse force, which deflects the motion of the atomic cloud (see Fig. 6). The direction in which the center of the cloud is deflected depends on the sign of $\sigma_{xy}$. Similar effects can be studied in collective modes with higher angular momentum, such as the quadrupole mode (39). We note that density inhomogeneities due to the trapping potential will lead to a distortion of the atomic cloud during its oscillation in the trap. However, the effect of a sign change in $\sigma_{xy}$ should be visible even in the presence of these distortions.

## Discussion and Outlook

In this paper, we focused on vortex dynamics for the Bose–Hubbard model. We mapped the sectors corresponding to different integers $p$, which characterizes the Hall conductivity and vortex motion throughout the phase diagram. We found that, close to the Mott insulating phases, the sign of $\sigma_{xy}$ is reversed and vortices flow against the applied current.

Our results are obtained neglecting vortex–vortex interactions or disorder. We note, however, that there are an infinite number of particle-hole symmetric points in the zero temperature phase diagram: at the tip of every Mott lobe, and in between two adjacent Mott lobes. We saw that the latter necessarily slice the full phase diagram into an infinite number of different $p$ sectors. This underlying structure cannot be removed by the inclusion of vortex–vortex interactions or disorder. However, the transition lines are expected to change their exact location and to be smoothed out by these effects, as well as by finite temperature.

Incidentally, reversal of the Hall conductivity has been repeatedly measured in many strongly correlated electronic materials, including high-temperature superconductors (e.g., refs. 2–4). These experiments are beyond the direct applicability of our model. An extension to treat these materials is an interesting future direction. As discussed above, a clean verification of our predictions is possible in systems of cold atoms.

**ACKNOWLEDGMENTS.** We thank Assa Auerbach, Ehud Altman, Joseph Avron, Hans-Peter Büchler, Olexi Motrunich, Ian Spielman, and Ady Stern for fruitful discussions. Special thanks to Daniel Podolsky for his enlightening comments. N.H.L. acknowledges support by The Gordon and Betty Moore Foundation through Caltech's Center for the Physics of Information, National Science Foundation Grant PHY-0803371, and the Israel Rothschild Foundation. S.D.H. acknowledges support by the Swiss Society of Friends of the Weizmann Institute of Science. This research was supported in part by the National Science Foundation under Grant PHY05-51164.

1. Ziman JM (1972) *Principles of the Theory of Solids* (Cambridge Univ Press, London), pp 246–255.
2. Hagen SJ, Lobb CJ, Greene RL, Forrester MG, Kang JH (1990) Anomalous hall effect in superconductors near their critical temperatures. *Phys Rev B Condens Matter Mater Phys* 41:11630.
3. LeBoeuf D, et al. (2007) Electron pockets in the fermi surface of hole-doped high-tc superconductors. *Nature* 450:533–536.
4. LeBoeuf D, et al. (2011) Lifshitz critical point in the cuprate superconductor $yba_2cu_3o_y$ from high-field hall effect measurements. *Phys Rev B Condens Matter Mater Phys* 83:054506.
5. Wen X-G (1995) Topological orders and edge excitations in fractional quantum hall states. *Adv Phys* 44:405.
6. Jaksch D, Bruder C, Cirac JI, Gardiner CW, Zoller P (1998) Cold bosonic atoms in optical lattices. *Phys Rev Lett* 81:3108.
7. Jaksch D, Zoller P (2005) The cold atom hubbard toolbox. *Ann Phys* 315:52–79.
8. Fazio R, van der Zant H (2001) Quantum phase transitions and vortex dynamics in superconducting networks. *Phys Rep* 355:235–334.
9. Simanek E (1979) Effect of charging energy on transition temperature of granular superconductors. *Solid State Commun* 31:419–421.
10. Doniach S (1981) Quantum fluctuations in two-dimensional superconductors. *Phys Rev B Condens Matter Mater Phys* 24:5063.
11. Uemura YJ, et al. (1989) Universal correlations between $\mathbf{t}_c$ $\mathbf{n}_s/\mathrm{m}^*$ (carrier density over effective mass) in high-$\mathbf{t}_c$ cuprate superconductors. *Phys Rev Lett* 62:2317–2320.
12. Micnas R, Robaszkiewicz S, Kostyrko T (1995) Thermodynamic and electromagnetic properties of hard-core charged bosons on a lattice. *Phys Rev B Condens Matter Mater Phys* 52:6863–6879.
13. Mihlin A, Auerbach A (2009) Temperature dependence of the order parameter of cuprate superconductors. *Phys Rev B Condens Matter Mater Phys* 80:134521.
14. Fisher MPA, Weichman PB, Grinstein G, Fisher DS (1989) Boson localization and the superfluid-insulator transition. *Phys Rev B Condens Matter Mater Phys* 40:546–570.
15. Lin YJ, Compton RL, Jimenez-Garcia K, Porto JV, Spielman IB (2009) Synthetic magnetic fields for ultracold neutral atoms. *Nature* 462:628–632.
16. Cooper NR (2011) Optical flux lattices for ultracold atomic gases. *Phys Rev Lett* 106:175301.
17. Fisher MPA (1991) Hall effect at the magnetic-field-tuned superconductor-insulator transition. *Physica A* 177:553–560.
18. Haldane FDM, Wu Y-S (1985) Quantum dynamics and statistics of vortices in two-dimensional superfluids. *Phys Rev Lett* 55:2887–2890.
19. Ao P, Thouless DJ (1993) Berry's phase and the magnus force for a vortex line in a superconductor. *Phys Rev Lett* 70:2158–2161.
20. Oshikawa M (2000) Commensurability, excitation gap, and topology in quantum many-particle systems on a periodic lattice. *Phys Rev Lett* 84:1535–1538.
21. Paramekanti A, Vishwanath A (2004) Extending luttinger's theorem to $z_2$ fractionalized phases of matter. *Phys Rev B Condens Matter Mater Phys* 70:245118.
22. Capogrosso-Sansone B, Prokov'ef N, Svistunov B (2007) Phase diagram and thermodynamics of the three-dimensional bose-hubbard model. *Phys Rev B Condens Matter Mater Phys* 75:134302.
23. van Oosten D, van der Straten P, Stoof HTC (2001) Quantum phases in an optical lattice. *Phys Rev A* 63:053601.
24. Polkovnikov A, Altman E, Demler E, Halperin B, Lukin MD (2005) Decay of superfluid currents in a moving system of strongly interacting boson. *Phys Rev A* 71:063613.
25. Dorsey AT (1992) Vortex motion and the hall effect in type-ii superconductors: A time-dependent ginzburg-landau theory approach. *Phys Rev B Condens Matter Mater Phys* 46:8376–8392.
26. Macdonald AH, Girvin SM, Yoshioka D (1988) $t/u$ expansion for the hubbard-model. *Phys Rev B Condens Matter Mater Phys* 37:9753–9756.
27. Lindner N, Auerbach A, Arovas DP (2010) Vortex dynamics and hall conductivity of hard core bosons. *Phys Rev B Condens Matter Mater Phys* 82:134510.
28. Avron JE, Seiler R (1985) Quantization of the hall conductance for general, multiparticle schrödinger hamiltonians. *Phys Rev Lett* 54:259–262.
29. Lindner NH, Auerbach A, Arovas DP (2009) Vortex quantum dynamics of two dimensional lattice bosons. *Phys Rev Lett* 102:070403.
30. Simon B (1983) Holonomy, the quantum adiabatic theorem, and berry's phase. *Phys Rev Lett* 51:2167–2170.
31. Berry MV (1984) Quantal phase factors accompanying adiabatic changes. *Proc R Soc Lond A* 392:45–57.
32. Albuquerque A, et al. (2007) The alps project release 1.3: Open-source software for strongly correlated systems. *J Magn Magn Mater* 310:1187–1193.
33. Fukui T, Hatsugai Y, Suzuki H (2005) Chern numbers in discretized brillouin zone: Efficient method of computing (spin) hall conductances. *J Phys Soc Jpn* 74:1674–1677.
34. Huber SD, Theiler B, Altman E, Blatter G (2008) Amplitude mode in the quantum phase model. *Phys Rev Lett* 100:050404.
35. Simanek E (1980) Instability of granular superconductivity. *Phys Rev B Condens Matter Mater Phys* 22:459–462.
36. Sonin EB (1997) Magnus force in superfluids and superconductors. *Phys Rev B Condens Matter Mater Phys* 55:485–501.
37. Huber SD, Altman E, Büchler HP, Blatter G (2007) Dynamical properties of ultracold bosons in an optical lattice. *Phys Rev B Condens Matter Mater Phys* 75:085106.
38. Bakr WS, Gillen JI, Peng A, Fölling S, Greiner M (2009) A quantum gas microscope for detecting single atoms in a hubbard-regime optical lattice. *Nature* 462:74–80.
39. Jin DS, Ensher JR, Matthews MR, Wieman CE, Cornell EA (1996) Collective excitations of a Bose-Einstein condensate in a dilute gas. *Phys Rev Lett* 77:420–423.